HHS Public Access

Author manuscript

Biochim Biophys Acta Proteins Proteom. Author manuscript; available in PMC 2020 May 01.

Published in final edited form as:

Biochim Biophys Acta Proteins Proteom. 2019 May ; 1867(5): 519–528. doi:10.1016/j.bbapap.2018.11.007.

Lysophospholipids induce Fibrillation of the Repeat domain of Pmel17 through intermediate core-shell structures

Jannik Nedergaard Pedersen[1], **Zhiping Jiang**[2], **Gunna Christiansen**[3], **Jennifer C. Lee**[2], **Jan Skov Pedersen**[1,*], **Daniel E. Otzen**[*,4]

[1]Interdisciplinary Nanoscience Center (iNANO) and Department of Chemistry, Aarhus University, Gustav Wieds Vej 14, 8000 Aarhus C, Denmark

[2]Laboratory of Protein Conformation and Dynamics, Biochemistry and Biophysics Center, National Heart, Lung, and Blood Institute, National Institutes of Health, Bethesda, MD 20892-8013, USA

[3]Department of Biomedicine, Aarhus University, Wilhelm Meyers Allé 4, DK-8000 Aarhus, Denmark

[4]Interdisciplinary Nanoscience Center (iNANO), Department of Molecular Biology and Genetics, Aarhus University, Gustav Wieds Vej 14, DK – 8000 Aarhus C, Denmark

Abstract

Lipids often play an important role in the initial steps of fibrillation. The melanosomal protein Pmel17 forms amyloid *in vivo* and contains a highly amyloidogenic Repeat domain (RPT), important for melanin biosynthesis. RPT fibrillation is influenced by two lysolipids, the anionic lysophosphatidylglycerol (LPG) and zwitterionic lysophosphatidylcholine (LPC), both present *in vivo* at elevated concentrations in melanosomes, organelles in which Pmel17 aggregate. Here we investigate the interaction of RPT with both LPG and LPC using small-angle X-ray scattering (SAXS), isothermal titration calorimetry (ITC), electron microscopy, fluorescence and circular dichroism (CD) spectroscopy. Under non-shaking conditions, both lipids promote fibrillation but this is driven by different interactions with RPT. Each RPT binds > 40 LPG molecules but only weak interactions are seen with LPC. Above LPG's criticial micelle concentration (cmc), LPG and RPT form connected micelles where RPT binds to the surface as beads on a string with core-shell structures. Binding to LPG only induces α-helical structure well above the cmc, while LPC has no measurable effect on the protein structure. While low (but still super-cmc) concentrations of LPG strongly promote aggregation, at higher LPG concentrations (10 mM), only ~ one RPT binds per micelle, inhibiting amyloid formation. ITC and SAXS reveal some interactions between the zwitterionic lipid LPC and RPT below the cmc but little above the cmc. Nevertheless, LPC only promotes aggregation above the cmc and this process is not inhibited by high LPC concentrations, suggesting that monomers and micelles cooperate to influence amyloid formation.

GRAPHICAL ABSTRACT

*Correspondence to dao@inano.au.dk (D.E.O.) and jsp@chem.au.dk (J.S.P.).

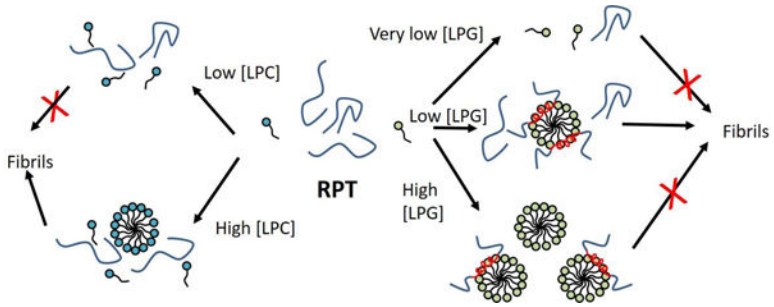

Keywords

pmel17; functional amyloid; lysolipid micelles; fibrillation; SAXS; ITC

1. INTRODUCTION

Many proteins can aggregate to form characteristic β-sheet-rich structures called amyloids. The phenomenon is so widespread that the amyloid structure is suggested to be a generic protein fold [1]. Amyloid is associated with diseases such as Alzheimer's, Parkinson's and various amyloidosis. However, the amyloid fold has also been shown to serve useful biological purposes in a wide range of organisms. In humans, amyloids are involved in melanosome formation, sperm selection, hormone storage and release and necrosome formation [2–5], while bacteria produce amyloid to strengthen biofilm and promote uptake into eukaryotes [6, 7] and fungi form transmissible prions with useful traits [8]. Although many proteins can aggregate spontaneously, cofactors can play a significant role in the aggregation process. While *in vivo* amyloid deposits typically have one major protein component, they also contain significant populations of other proteins (*e.g.* serum amyloid P and apolipoprotein E4), glycosaminoglycans, and metal ions [9]. Lipids also play a major role in amyloid formation. Anionic lipids can trigger aggregation of otherwise stable globular proteins [10] and conversely, the process of amyloidogenesis can trigger major changes in the membrane with deleterious consequences such as uncontrolled leakage of vesicle contents [11, 12]. Protein-lipid interactions and their mechanistic ramifications are therefore crucial to understand. This is particularly the case for intrinsically disordered proteins such as α-synuclein involved in Parkinson's Disease, where binding to membranes often induces formation of isolated α-helices [13]. Such semi-structured forms may be important for aggregation [14].

Fibrillation of the human protein Pmel17 [3] is critical for melanin deposition *in vivo* [15]. Pmel17 is a transmembrane protein which is cleaved by a furin protease in the melanosome to release a peptide consisting of residues 25–467 that serves as a structural scaffold for melanin [16]. The synthesis of melanin is suggested to occur on fibrils formed of this peptide and the fibril provides a detoxifying environment for the otherwise toxic melanin [16]. Within this peptide, the intrinsically disordered repeat domain (RPT), consisting of residues 315–444 [17], turns out to be critical for amyloid formation [18]. The melanosomes are slightly acidic (pH 5). RPT fibrillation is highly pH-sensitive *in vitro*, with rapid fibrillation at pH 4–5 while fibrils dissolve at pH 6 and above [19, 20]. Residue E422 is

critical in controlling the pH sensitivity with mutants (E422Q and E422A) of this residue being able to form as high as pH 6.5 [21]. Both Pmel17 trafficking and its proteolytic fragmentation are important for amyloid formation [22]. In addition, the presence of lipids is important and formation of fibrils is thought to be initiated on intraluminal membrane vesicles [23]. Lysophospholipids constitute up to 10% of the total lipid composition at the melanosomal membrane [24] (in contrast to the plasma membrane where they generally make up < 2% of the lipid population) and strongly influence fibrillation of RPT *in vitro* [25]. Thus, the negatively charged lysolipid, lysophosphatidylglycerol (LPG, here with a C16 palmitoyl chain as the hydrophobic moiety) greatly accelerates fibrillation by decreasing nucleation times at low concentrations but inhibits fibrillation at high concentrations [25]. In contrast the zwitterionic lysophosphatidylcholine (LPC, here with a C12 lauroyl chain) accelerates fibrillation at all concentrations [25]. Unlike diacylated phospholipids, lysolipids do not form vesicles by themselves. Rather, they behave as surfactants that associate into micelles; the loss of one of the two acyl chains makes it unfavourable to pack lysolipids into bilayer structures. Micelles are much smaller than vesicles, making them more amenable to structural analysis by spectroscopy and small-angle X-ray scattering (SAXS).

Here, we extend the initial study of the interaction between RPT and the two lysolipids LPG (with a C16 palmitoyl chain) and LPC (with a C12 lauroyl chain) [25] (Fig. 1) by a combination of pyrene fluorescence, isothermal titration calorimetry (ITC), and SAXS to obtain more detailed information about the structure of the complexes formed between RPT and lysolipids. In the absence of lysolipids and without shaking, RPT does not fibrillate after 10 days, highlighting the importance of surface interactions provided by these lysolipids for RPT amyloid formation. RPT binds to the LPG micelle surface according to our SAXS studies. Consequently, RPT concentrations in the micelle phase increase at low LPG concentrations. In contrast, as the number of micelles increases at high LPG concentrations, the RPT population redistributes amongst them, leaving one RPT or less bound per micelle. By visual inspection we determine LPG to have a cmc of 9 ± 3 μM which is much smaller than the 0.6 mM reported in an earlier study where the salt concentration was not taken into account [25]. Furthermore, RPT does not alter the apparent cmc of LPG. Altogether this suggests that previous assumptions that LPG micelles inhibit RPT amyloid formation should be re-evaluated [25]. LPC only shows weak interactions with RPT, but still promotes amyloid formation, probably through a combination of monomeric and micellar LPC.

2. MATERIALS AND METHODS

2.1 Materials:

1-palmitoyl-2-hydroxy-sn-glycero-3-phospho-(1´-rac-glyceerol) (sodium salt) (LPG) and 1-lauroyl-2-hydroxy-sn-glycero-3-phosphocholine (LPC) were from Avanti Polar lipids, Inc. (Alabaster, AL). Guanidinium hydrochloride was from MP Biomedicals (Solon, OH). All other chemicals were from Sigma Aldrich (St. Louis, MO).

2.2 Protein expression and purification:

RPT was expressed and purified as previously described [25]. Before measurements, the buffer was exchanged (20 mM NaOAc, pH 5.0 and 100 mM NaCl) by filtering RPT with a PD-10 column (GE Healthcare). An Amicon Ultra 100K centrifugal filter from MERCK KGaM (Germany) was used to remove any preformed aggregates.

2.3 Aggregation kinetics:

Sealed 96-well flat-bottom plates were loaded with 200 μl sample per well and fibril formation followed by excitation of ThT at 415 nm and emission at 480 nm. For experiments with shaking, 2-mm sterile glass beads were added to the solution and measurements performed at 37 °C with 1 mm orbital shaking on a microplate reader (Tecan Infinite M200 Pro). All samples were in quartets. Non-shaking fibrillation measurements were performed in 96-well flat bottom plates from Corning (Kennebunk, ME) at 25 °C on either a Varioskan Flash Multimode Reader from Thermo Scientific (Waltham, MA) or a CLARIOstar from BMG labtech (Germany) and were done in triplets.

2.4 Pyrene binding:

The critical micelle concentration (cmc) of LPG and LPC was estimated by excitation of pyrene at 335 nm and emission at 383 nm (I_3) and 372 nm (I_1) on a LS-55 Luminescence spectrometer from Perkin Elmer (UK). As pyrene partitions into the hydrophobic environment of a micelle interior, the ratio of emission at 383 and 372 nm changes [26]. Pyrene was added to a final concentration of 0.2 μM (0.5 % EtOH) in 20 mM NaOAc, pH 5.0 and 100 mM NaCl. A sample containing pyrene and 30 μM RPT was used to investigate if RPT changed the cmc of LPG or LPC. Intensities and concentrations have been corrected for dilution. The cmc values from pyrene were compared to those determined with ITC and an average as well as standard deviation was determined from the two values.

2.5 Circular dichroism (CD):

72 μM RPT was incubated with 0–10 mM LPG in 20 mM NaOAc, pH 5.0 and 100 mM NaCl for 0 or 10 days and CD was recorded on a Chirascan Plus (Applied Photophysics Ltd, Surrey, UK) at ambient temperature. 0.1 mm quartz crystal cuvettes were used to measure in the range of 190 to 250 nm with a bandwidth of 1 nm. The buffer was subtracted from the data and the average of three measurements is shown.

2.6 SDS-PAGE:

Samples from the aggregation kinetics experiments that had incubated >10 days without shaking were spun at 12,100 g for 8 min. The supernatant was mixed with a reducing loading buffer and heated to 95 °C for 5 min before being loaded on a 15% BisTris SDS-PAGE gel. The gel was stained with Coomassie Brilliant Blue.

2.7 Transmission electron microscopy:

Five μl of endpoint samples from the non-shaking ThT assay (72 μM or 30 μM RPT with 0, 0.1, 0.5 or 10 mM LPG) were mounted on carbon coated, glow discharged 400 mesh Ni grids (Gilder, Grantham, UK) for 1 min, stained with one drop of 1% phosphotungstic acid

(PTA) pH 7.0 for 30 sec. and blotted dry on filter paper. Electron microscopy was done on a JEOL 1010 transmission electron microscope (JEM 1010, Tokyo,Japan) operated at 60 keV. Electron micrographs were recorded using an electron-sensitive CCD camera (KeenView, Olympus, Tokyo, Japan). For size determination, a grid-size replica (2,160 lines/mm) was used.

2.8 Small-angle X-ray scattering:

RPT was measured at a concentration of 1 mg/ml (72 μM) with 0–10 mM LPG presence in 20 mM NaOAc, pH 5.0 and 100 mM NaCl. Measurements were done at 25 °C with an acquisition time of 10 min. Measurements were done on an optimized NanoSTAR SAXS instrument [27] from Bruker AXS installed at Aarhus University equipped with scatterless pinholes [28] and a liquid Ga metal jet X-ray source (Excillum) [29]. The data is shown as a function of the scattering vector q that is dependent on the scattering angle 2θ with $q = 4\pi/\lambda \sin\theta$, where $\lambda = 1.34$ Å. The SUPERSAXS program package (Oliveira, C.L.P. and Pedersen J.S, unpublished) was used to make background subtraction and convert data to absolute scale with water as a calibration standard. RPT on its own has little structure and we fitted the data with the random coil model obeying Gaussian statistics of Debye [30]. The LPG micelles were modelled as a core-shell oblate ellipsoid. The volume of the tail of LPG was calculated from [31] and electron densities of $\rho_{tail} = 0.281$ e Å^{-3} and $\rho_{head} = 0.470$ e Å^{-3} were used [32]. For the complex of RPT and LPG we use a model of beads-on-a-string chain similar to that used for SDS-α-synuclein complexes [33]. Here, we use a core-shell model with the core consisting of the LPG tail and the shell consisting of the LPG headgroups, RPT and water. Fitting was done on absolute scale using absolute protein and lipid concentrations. The core radius r_{core}, shell thickness D_{Head}, the eccentricity of the micelle ε and the number of micelles $N_{micelles}$ in a beads-on-a-string cluster, were all fitting parameters. The distance between core-shell structures in a cluster was set to twice the radius of the core-shell structure. For high and low LPG concentrations, a term describing the scattering from free LPG micelles or free proteins had to be added, respectively, to fit the data. This contribution was added as a background contribution from the pure LPG and RPT samples.

2.9 Isothermal titration calorimetry (ITC):

Binding of LPG or LPC to RPT was monitored with a VP isothermal titration calorimeter from MicroCal (MA, USA). A solution of 21 mM lysolipid in 20 mM NaOAc, pH 5.0 and 100 mM NaCl was titrated into 0–50 μM RPT in 20 mM NaOAc, pH 5.0 and 100 mM NaCl at 25 °C. One initial injection of 2 μl was followed by 10 μl injections. For determination of cmc of lysolipid, a solution of 3 mM lysolipid in 20 mM NaOAc, pH 5.0 and 100 mM NaCl was titrated into 20 mM NaOAc, pH 5.0 and 100 mM NaCl at 25 °C. All solutions were degassed before use. The Origin software from MicroCal was used to integrate the raw heat signals. The three transition points of LPG titration in RPT were determined by (1) locally fitting the data to a polynomial, (2) determining the point at which the signal (enthalpy of injection) was half way back to 0 kcal/mol and (3) intersect between straight line going through (2) and straight line going through 0 kcal/mol. Bound and free LPG in the transition points was determined by the relationship $[LPG]_{tot} = [LPG]_{free} + [LPG]_{bound}$ [RPT].

3. RESULTS

3.1 C16-LPG has a much lower cmc than C12-LPC

The single most important parameter defining surfactants such as LPG and LPC is their critical micelle concentration (cmc), *i.e.* the concentration at which they start to form micelles. Monomers and micelles usually differ greatly in their interaction with proteins [34], so measurements above and below the cmc provide insight into the nature of protein-LPG interactions. LPG's cmc in water is 0.6 mM [35]. However, cmc is sensitive to buffer conditions, and we therefore tested how the cmc of LPG is affected by our buffer. The buffer consists of20 mM NaOAc and 100 mM NaCl pH 5.0, mimicking the low pH of melanosomes with a salt concentration close to that of physiological conditions. We titrated LPG into buffer and monitored the process by ITC. The cmc was estimated from the intercept between baseline and the transition zone, giving a value of ~ 7 μM, *i.e.* a ca. 100-fold decrease in value compared to that in water (Fig. 1A). The decrease in cmc is to be expected; since LPG is negatively charged, the addition of salt will screen the lipid head group repulsion and thus favour micelle formation. However, the magnitude of the effect is remarkable; the anionic surfactant SDS only undergoes a 10-fold decrease in cmc when going from water to PBS buffer containing 150 mM NaCl [36]. Nevertheless, the low cmc value is supported by an alternative approach, namely pyrene fluorescence that leads to a cmc of 11 μM (Fig. 1B). The cmc did not change in the presence of 30 μM RPT. This indicates that RPT does not promote micelle formation of LPG through binding of LPG monomers, but only interacts with the micelle.

Based on ITC and pyrene fluorescence we estimate the cmc of LPC to be 0.37 ± 8 mM (Fig. 1A), in good agreement with previously reported values of 0.43 mM [37] and 0.6 mM [38]. The higher cmc of LPC compared to LPG may be rationalized by the longer alkyl chain length of LPG (C16 versus C12 for LPC) combined with the reduction in LPG's head group repulsion by salt. Pyrene fluorescence show that RPT does not affect the cmc of LPC, indicating that LPC, like LPG, does not form micellar clusters on RPT below the cmc (Fig. 1B).

3.2 RPT aggregation kinetics saturate above 2 μM in the absence of lysolipids

To investigate the aggregation mechanism of RPT in the absence of LPG and LPC, we incubated RPT at different concentrations and monitored the process with the amyloid-binding dye thioflavin T (ThT) (Fig. 2A). This was done under shaking conditions to ensure RPT fibrillation occurred and to be able to compare to earlier fibrillation studies done at similar conditions [25]. An increase in ThT signal over time was seen for RPT concentrations of 1 μM and above. The end level of ThT scaled nonlinearly with RPT concentration (Fig. 2A **insert**). When we normalize the ThT time profiles by setting end and start values to 100 and 0%, respectively, it is clear that the lag phase is essentially constant between 5 and 80 μM RPT (consistent with previous reports [20]) and only increases around 1–2 μM. Furthermore, the elongation rate (*i.e.* the slope of the transition zone between the start and end base lines) did not change with RPT concentrations above 5 μM, suggesting that it could involve concentration-independent steps (or was already saturated at 5 μM RPT). In addition, there was a small increase in signal within the first 10 hours at higher

concentrations, which accounted for < 20% of the total increase in signal. The lack of concentration dependence in lag and elongation phases prevents a kinetic analysis of the mechanism of aggregation using *e.g.* the formalism of the Amylofit programme [39] and suggests that the rate-limiting steps in fibrillation could involves concentration-independent conformational changes above a certain critical aggregation concentration, cf. [20].

3.3 Aggregation depends on the LPG:RPT ratio rather than the absolute LPG concentration

LPG is known to accelerate RPT fibril formation at low concentrations and block fibril formation at high concentrations [25]. We tested whether this effect depended on absolute LPG concentrations or LPG:RPT ratios by following fibrillation at two RPT concentrations (32 and 72 μM) and 0.1–10 mM LPG (Fig. 2B and C). In both cases, low concentrations of LPG (up to 1–3 mM) strongly reduced the lag phase of fibrillation while higher concentrations reduce the end-point level of ThT fluorescence (*i.e.* the amount of fibrillated protein) and also increase the lag time. Increasing the RPT concentration from 32 μM to 72 μM increased the LPG concentration needed to reduce fibrillation to 50% of the maximal value from ca. 0.5 mM (32 μM RPT) to ca. 1.5 mM (72 μM RPT))(Fig. 2D). The effect of LPG on RPT is thus dependent on the ratio between RPT and LPG rather than the total LPG concentration.

3.4 LPG promotes fibrillation within a narrow concentration range while LPC promotes fibrillation above its cmc

To obtain insight into the structural changes accompanying fibrillation of RPT in the presence of LPG, we first investigated the effect of LPG on RPT fibrillation in the absence of shaking (Fig. 3A–B and E). Shaking is known to induce fibrillation and decrease the lag phase [40, 41]. Conversely, removal of shaking should strongly slow down fibrillation and this is also observed for RPT. Experiments of 2 mg/ml RPT in absence of shaking has shown fibrillation times of weeks to months [18]. Under our experimental conditions, fibrillation is completely prevented in absence of LPG over a period of 10 days, highlighting the importance of shaking for this process. No fibrillation was seen at 10 mM LPG (Fig. 3A–B and E), consistent with the strong decrease in ThT signal under shaking conditions. Intermediate LPG concentrations induced fibrillation (although much more slowly than when shaking), suggesting that an interface is needed for RPT fibrillation that can be provided by the water-air interface during shaking or by the LPG micellar surface. We also investigated the effect of LPC under non-shaking conditions (Fig. 3C–E) and found, consistent with earlier findings [25], that LPC has no effect on fibrillation of RPT below the cmc (cmc = 0.43 mM [37]) but only has an effect above the cmc. For the low RPT concentration of 30 μM similar aggregation behavior is seen in presence of 0.75–20 mM LPC while 0–0.5 mM LPC has no effect in the measured time. For 72 μM RPT, there is a progressively decreasing lag time as we go from 0.75 to 20 mM LPC. This may be related to the limited amount of monomeric LPC present to bind to RPT to “prime” it for aggregation similar to what is seen for LPG (see below).

After 10 days of incubation, samples were investigated by circular dichroism (CD), SDS-PAGE and electron microscopy (EM). Far-UV CD monitors the changes in secondary

structures caused by the presence of LPG both before and after fibril formation. Monomeric RPT is largely disordered, as seen by the CD profile with a minimum around 200 nm (Fig. 3F). With increasing concentrations of LPG, the spectrum transitions to an α-helix-dominated profile with two new minima at 222 and 208 nm at 10 mM LPG (Fig. 3F). After incubation at ambient temperature for 10 days, samples containing 0.1–3 mM LPG have all undergone a large decrease in spectral intensity, probably due to precipitation of the protein as fibrils (Fig. 3G).

However, the spectra are very broad and show minima around 218 nm, consistent with β-sheet structure. At 0 and 10 mM LPG, no changes are seen, in good agreement with the lack of ThT signal in the fibrillation assay. LPC did not have any effect on the CD signal of RPT at any concentration tested (data not shown). To confirm that fibrils are mainly formed at intermediate LPG concentrations, we measured the amount of soluble material, *i.e.* supernatant after centrifugation, by SDS-PAGE (Fig. 3H). Relative to a monomeric control, samples with 0 and 10 mM LPG (which did not produce a ThT signal) had 108% and 92% protein in the supernatant, respectively. With 0.1 and 0.5 mM LPG, only 54% and 16% of RPT was left in the supernatant, respectively, suggesting formation of insoluble aggregates such as fibrils at these concentrations. Transmission electron microscopy (TEM) confirmed the presence of fibrils at 0.1–0.5 mM LPG as large networks of thin fibers (Fig. 4). At 0 mM LPG, mostly monomers was present but also smaller RPT aggregates could be observed. At 10 mM LPG, a large amount of monomers and large round structures was seen but only very few fibrils.

3.5 RPT binds more than 40 LPG per RPT, but little specific binding of LPC to RPT is detected

To detect individual LPG-RPT binding steps and LPG:RPT binding stoichiometry we turned to ITC. Titrating LPG into different concentrations of RPT provided enthalpograms, which allows us to estimate binding numbers and the ratios with the highest enthalpy changes (Fig. 5A–C). Higher concentrations of RPT shifted these titration curves to higher concentrations of LPG, indicating that more LPG was needed to reach a certain level of binding at higher RPT concentrations. We selected three characteristic points from the titration curves (Fig. 5B) and used the previously established mass balance equation ($[LPG]_{tot} = [LPG]_{free} + [LPG]_{bound}$ [RPT]) [42] to determine the amount of bound and free LPG at these points (Table 1). The largest enthalpy change (transition point 1) was seen when 21±3 LPG bound per RPT molecule. At Point 2 (halfway between Point 1 and baseline at 0 kcal mol^{-1}) and Point 3 (intercept of the two last linear regions in Fig. 5B), we determined LPG:RPT binding ratios of 36±6 and 41±7, respectively. LPG's low cmc (~7 μM) means that all titrations were above the cmc and only a small amount (0.2–0.4 mM) of free LPG was seen at Points 1–3 (Table 1). In contrast to the distinct binding profile of LPG, titrating LPC into different concentrations of RPT (Fig. 5D) showed little difference between having RPT absent or present in solution, and the little change that was seen took place below LPC's cmc, indicating weak interactions between RPT and monomeric LPC.

3.6 LPG-RPT forms core-shell structures while no distinct complexes are formed between LPC and RPT

We finally turned to small-angle X-ray scattering (SAXS) to monitor the changes in structure of the LPG-RPT complexes in connection with fibrillation. We first studied LPG-free RPT and found that the protein showed a typical unfolded polymer scattering pattern (Fig. 6A). It was possible to fit the data on absolute scale to a random coil model ($\chi^2 = 1.0$) with a radius of gyration R_g of 4.00 ± 0.04 nm and a molecular weight of 13.9 ± 0.4 kDa, in good agreement with monomeric RPT's known molecular weight of 13.9 kDa. Free LPG showed a characteristic micellar "bump" with a sharp minimum around 0.09 $Å^{-1}$ and maximum at 0.14 $Å^{-1}$. The data could be fitted by a micelle in the shape of an oblate ellipsoid (Fig. 6A) with an eccentricity of 0.65 and an aggregation number of 95 (Table 2).

Mixtures of 72 μM RPT and 0–10 mM LPG were also investigated (Fig. 6B) and with increasing concentrations showed a "bump" at 0.14 $Å^{-1}$ similar to that of the free micelle. All samples were fitted with the same model on absolute scale, in which a core consisting of the LPG micelle is decorated with RPT. According to Table 1, the three characteristic points in the binding curve of Fig. 5 take place at 1.64–3.26 mM LPG in the presence of 72 μm RPT. Thus, the SAXS data are recorded under conditions where we either have a large excess of free RPT at low [LPG] (0.1–1 mM, before Point 1) or a large excess of free LPG at high LPG concentrations (mainly 10 mM, beyond Point 3). Therefore we included the scattering from, respectively, free monomeric RPT and free micellar LPG in our fitting. These contributions were represented by actual measured experimental data sets. In our model, micelle-bound RPT is partially unstructured as seen by a shell thickness of approximately 2 nm and can potentially interact with several micelles to form a beads-on-a-string cluster as also seen for sodium dodecyl sulfate [33] and oleic acid [43] micelles. This model fitted the data on an absolute scale for all the mixtures with $\chi^2 < 1.5$. For the solutions with 10 mM LPG, a contribution of free micelles was added while this was negligible for the rest of the solutions. At 0.1–1.0 mM LPG a contribution from free protein was added. At 10 mM LPG ~1 PRT on average was bound per complex, typically spread out on 1–2 micelles. As the concentration of LPG decreased, both the number of bound RPT per complex and the number of micelles per complex increased.

The fibrillation of RPT at different LPG concentrations was also followed with SAXS over time. However, upon aggregation, the signal rapidly increased at low q and the formed structures were larger than what would have been expected for regular fibrils in solution (Data not shown). We attribute this to the networking structure of the fibrils seen with TEM. These data are also consistent with the decrease of ThT signal over time (Fig. 2B–C) which could be indicative of rearrangements of the fibrils into larger clusters that reduce binding of ThT. We were not able to determine if LPG or LPC was integrated in the final fibrils.

Finally, we investigated mixtures of RPT with increasing LPC concentrations (Fig. 6C). At the lowest investigated concentration of 0.5 mM LPC, the signal was very similar to that of free unfolded protein except for a large upturn in intensity at low q, consistent with a certain degree of aggregation in solution. As the LPC concentration was increased, a clear bump around 0.14$Å^{-1}$ and a broad peak around 0.05$Å^{-1}$ were observed, both of which stem from the LPG curve. The scattering curves for RPT with 1–10 mM LPC could all be fitted by a

linear combination of the the curves for RPT in the presence of 0.5 mM LPC and free LPC micelles, suggesting that the LPC micelles do not interact significantly with RPT which rather has a low degree of association with monomeric LPC, leading to a certain degree of clustering.

4. DISCUSSION

In the following two sections we discuss the picture that emerges from our data in terms of how LPG and LPC drive fibrillation of RPT. This picture is summarized in Fig. 7.

4.1 LPG micelles both drive and inhibit RPT fibrillation

Negatively charged LPG is able to both accelerate and halt fibrillation of the human functional amyloid RPT [25]. Since RPT does not change the apparent cmc of LPG, we conclude that RPT interacts with micellar but not monomeric LPG. Because of LPG's low cmc (~0.01 mM), only a very small amount of LPG is accessible in its monomeric form, corresponding to 1 LPG:7RPT at 1 mg/ml RPT. Fibrillation at two different RPT concentrations and several different LPG concentrations show that more LPG is needed to inhibit fibrillation at high RPT concentrations compared to low concentrations. This suggests that the interaction between LPG and RPT is likely to occur between micelles and protein, and the rate limiting parameter is the ratio between LPG and RPT.

Inhibition of fibrillation for 30 μM RPT occurs at 1–3 mM LPG while it happens at 3–10 mM LPG for 72 μM RPT (Fig. 2B–C). From ITC it is seen that saturation of the RPT-LPG interaction (point 3) occurs at 1.6 mM and 3.3 mM LPG for 30 and 72 μM RPT, respectively. This saturation is also seen for SAXS at 72 μM RPT where only 4.2±0.5 – 4.9±0.5 mM LPG is bound at the highest LPG concentrations (Table 2) and fibril inhibition therefore seems to be closely related to saturation of LPG-RPT binding. SAXS show that several RPT monomers at low and intermediate LPG concentrations bind a single micelle (Table 2), thereby increasing the local RPT concentration and increasing the likelihood of nucleation events. Furthermore, the micelles also seems to induce helical structure in RPT (Fig. 2E) which could also be important for the aggregation since structured forms of intrinsically disordered proteins are known to contribute to aggregation [14]. On the other hand, removal of α-helical structure in the islet amyloid polypeptide has been shown to enhance fibrillation [44] suggesting that the α-helical structure might also contribute in stabilizing the monomer structure of intrinsically disordered proteins. At high LPG concentrations, all RPT is bound to micelles with approximately one RPT per complex (Table 2). The depletion of free RPT likely stalls fibrillation, since electrostatic repulsion between anionic micelles will prevent association of LPG-bound RPT (the essentially neutral state of RPT, whose p*I* is 4.5–5.5 depending on the aggregation state [15], will not neutralize the negative charge of the LPG micelles).

Fibrillation kinetics of lipid-free RPT converges above 2 μM (Fig. 2A) and suggests that the kinetics are limited by either concentration-independent changes (such as nucleated conformational conversion [45, 46] of a cluster of molecules that are formed rapidly in a phase-separation step) and/or access to an interface where nucleation can occur or the cluster can mature to fibrils. This is also seen for other systems such as α-synuclein interaction with

lipid surfaces [47] or the air-water interface [48, 49]. RPT clusters are not detected in lysolipid-free RPT SAXS data but may be present at levels insufficient for detection. The lack of RPT fibril formation in the absence of lipids and shaking (Fig. 3A and B) further suggests that lipids may promote RPT fibrillation by destabilizing such clusters and presenting alternative binding places for the RPT molecules, effectively hijacking the aggregation pathway. The presence of large amounts of soluble RPT (54 %) after fibrillation in the presence of 0.1 mM LPG suggests that fibrillation is not stopped simply by depleting soluble monomer. It may be instructive to consider the behaviour of α-synuclein, which also shows incomplete fibrillation in the presence of lipids. In this case, fibrillation of the remaining α-synuclein monomer was shown to be initiated by sonication or addition of more lipid [47], suggesting that fragmentation and/or the presence of accessible interfaces were limiting factors. By analogy, the termination of fibrillation of the remaining monomeric RPT in the LPG solution could be caused by depletion of nucleation sites on LPG micelles and inactivation of growing fibrils. At 0.5 mM LPG only 16% RPT remained in solution after fibrillation and the increased amount of LPG has likely increased the possible nucleation sites for RPT fibrillation.

In a study of the interaction of α-synuclein with SDS it was shown that the formed complex consists of a core of SDS surrounded by α-synuclein with several of these structures clustering together [33]. The structure of the RPT-LPG complex is very similar to this and the aggregation kinetics of the SDS-α-synuclein complex also only show fibril formation at an optimum concentration of SDS. The mechanism is likely to be similar to that of RPT since SDS and LPG both are negatively charged and both proteins form α-helical structures on the surface of the lipids.

The C-terminus of RPT contains a small stretch predicted to have α-helical structure propensity [25] and at the same time this region has amino acids that are part of the amyloid core [21]. Inhibition of fibril formation could therefore also be influenced by burial of amino acids upon interaction with LPG and α-helical formation. However, α-helical structure does not seem to inhibit fibril formation as long as some RPT is free in solution. The C-terminal contains a glutamic acid, E422, that has been shown to greatly accelerate fibrillation when the charge is neutralized [21] and incorporation of E422 into a lipid environment could potentially favour the protonated state and thereby effect fibrillation. This highlights the importance of the negative charge of LPG in driving RPT's structural change and inhibiting fibrillation.

4.2 LPC-driven fibrillation: cooperation between monomers and micelles?

The zwitterionic lysolipid, lysophosphatidylcholine (LPC) also increases the fibrillation rate but has a higher cmc than LPG (0.4 mM compared to 0.01 mM for LPG) [25]. LPC does not seem to promote α-helical structure in RPT nor does it inhibit fibrillation at high concentrations [25]. Interestingly, neither SAXS nor ITC measurements detect interactions between LPC and RPT above the cmc, even though effects on fibrillation are only observed above the cmc according to our ThT assay. This suggests that promotion of fibrillation requires both monomers and micelles of LPC to be present in solution. In the case of α-lactalbumin, unfolding with nonionic and zwitterionic surfactants, monomers and micelles

have also been suggested to cooperate in the unfolding process [50]; unfolding rates saturated slightly above the cmc and the rates decreased with chain length, indicating that the greater the cmc (and thus the greater the concentration of monomeric species), the faster the protein could unfold once micelles were present. The monomers were suggested to "soften" α-lactalbumin by altering its conformation in a way that promoted interactions with micelles. A similar mechanism might be at play with RPT, although the effect will likely be more subtle since no gross change in secondary structure was detected by CD. Further elucidation of this phenomenon will require comparison of fibrillation kinetics in the presence of LPC lysolipids of different chain lengths and consequently different cmc values, though this is outside the scope of the present investigation.

5. SUMMARY

We have studied the amyloid formation of the functional amyloid RPT in the presence of lysophospholipids. Micelles of the ionic lipid LPG interacts strongly with RPT and forms a core-shell structure with a beads-on-a-string-like arrangement that enhances fibrillation at low concentrations and a core-shell structure that inhibits fibrillation at high concentrations. Micelles of the zwitterionic lipid LPC show no interaction when studied with SAXS and ITC while some interaction might occur below the cmc. Since LPC only enhances fibrillation above the cmc it could suggest that some weak interactions between LPC and RPT might still be present. These results can give insight into how lysophospholipids might influence RPT aggregation and can give some understanding of general protein-lipid interactions of amyloidogenic proteins.

ACKNOWLEDGEMENT

We would like to thank Dr. Maria Andreasen for valuable discussions. The support from the Danish Independent Research Foundation | Natural Sciences (grant 4002–00479) and the Danish Independent Research Foundation | Technical Sciences (grant 4184–00218) is gratefully acknowledged. ZJ and JCL is supported by the Intramural Research Program at the National Institutes of Health, National Heart, Lung, and Blood Institute.

Abbreviations

CD	circular dichroism
cmc	critical micelle concentration
ITC	Isothermal titration calorimetry
LPC	lysophosphatidylcholine
LPG	lysophosphatidylglycerol
OA	oleic acid
R_g	radius of gyration
RPT	repeat domain
SAXS	small-angle X-ray scattering

SDS	sodium dodecyl sulfate
TEM	transmission electron microscopy
ThT	thioflavin T

REFERENCES

[1]. Dobson CM, Protein misfolding, evolution and disease., TIBS, 24 (1999) 329–332. [PubMed: 10470028]

[2]. Li J, McQuade T, Siemer AB, Napetschnig J, Moriwaki K, Hsiao YS, Damko E, Moquin D, Walz T, McDermott A, Chan FK, Wu H, The RIP1/RIP3 necrosome forms a functional amyloid signaling complex required for programmed necrosis, Cell, 150 (2012) 339–350. [PubMed: 22817896]

[3]. Fowler DM, Koulov AV, Alory-Jost C, Marks MS, Balch WE, Kelly JW, Functional amyloid formation within mammalian tissue, Plos Biol, 4 (2006) 100–107.

[4]. Maji SK, Perrin MH, Sawaya MR, Jessberger S, Vadodaria K, Rissman RA, Singru PS, Nilsson KPR, Simon R, Schubert D, Eisenberg D, Rivier J, Sawchenko P, Vale W, Riek R, Functional Amyloids As Natural Storage of Peptide Hormones in Pituitary Secretory Granules, Science, 325 (2009) 328–332. [PubMed: 19541956]

[5]. Roan NR, Sandi-Monroy N, Kohgadai N, Usmani SM, Hamil KG, Neidleman J, Montano M, Standker L, Rocker A, Cavrois M, Rosen J, Marson K, Smith JF, Pilcher CD, Gagsteiger F, Sakk O, O'Rand M, Lishko PV, Kirchhoff F, Munch J, Greene WC, Semen amyloids participate in spermatozoa selection and clearance, eLife, 6 (2017).

[6]. Barnhart MM, Chapman MR, Curli biogenesis and function, Annu Rev Microbiol, 60 (2006) 131–147. [PubMed: 16704339]

[7]. Chapman MR, Robinson LS, Pinkner JS, Roth R, Heuser J, Hammar M, Normark S, Hultgren SJ, Role of Escherichia coli curli operons in directing amyloid fiber formation, Science, 295 (2002) 851–855. [PubMed: 11823641]

[8]. Maddelein ML, Dos Reis S, Duvezin-Caubet S, Coulary-Salin B, Saupe SJ, Amyloid aggregates of the HET-s prion protein are infectious, Proc Natl Acad Sci U S A, 99 (2002) 7402–7407. [PubMed: 12032295]

[9]. Chiti F, Dobson CM, Protein Misfolding, Amyloid Formation, and Human Disease: A Summary of Progress Over the Last Decade, Annu Rev Biochem, 86 (2017) 27–68. [PubMed: 28498720]

[10]. Zhao H, Tuominen EK, Kinnunen PK, Formation of amyloid fibers triggered by phosphatidylserine-containing membranes, Biochemistry, 43 (2004) 10302–10307. [PubMed: 15301528]

[11]. Relini A, Cavalleri O, Rolandi R, Gliozzi A, The two-fold aspect of the interplay of amyloidogenic proteins with lipid membranes, Chem Phys Lipids, 158 (2009) 1–9. [PubMed: 19056366]

[12]. Engel MF, Khemtemourian L, Kleijer CC, Meeldijk HJ, Jacobs J, Verkleij AJ, de Kruijff B, Killian JA, Hoppener JW, Membrane damage by human islet amyloid polypeptide through fibril growth at the membrane, Proc Natl Acad Sci U S A, 105 (2008) 6033–6038. [PubMed: 18408164]

[13]. Kjær L, Giehm L, Heimburg T, Otzen DE, The influence of vesicle composition and size on α-synuclein structure and stability, Biophys. J, 96 (2009) 2857–2870. [PubMed: 19348768]

[14]. Zhang T, Faraggi E, Li Z, Zhou Y, Intrinsically semi-disordered state and its role in induced folding and protein aggregation, Cell Biochem Biophys, 67 (2013) 1193–1205. [PubMed: 23723000]

[15]. Raposo G, Marks MS, Melanosomes--dark organelles enlighten endosomal membrane transport, Nat Rev Mol Cell Biol, 8 (2007) 786–797. [PubMed: 17878918]

[16]. McGlinchey RP, Lee JC, Reversing the amyloid trend: Mechanism of fibril assembly and dissolution of the repeat domain from a human functional amyloid, Isr J Chem, 57 (2017) 613–621. [PubMed: 28993712]

[17]. Hoashi T, Muller J, Vieira WD, Rouzaud F, Kikuchi K, Tamaki K, Hearing VJ, The repeat domain of the melanosomal matrix protein PMEL17/GP100 is required for the formation of organellar fibers, Journal of Biological Chemistry, 281 (2006) 21198–21208. [PubMed: 16682408]

[18]. McGlinchey RP, Shewmaker F, McPhie P, Monterroso B, Thurber K, Wickner RB, The repeat domain of the melanosome fibril protein Pmel17 forms the amyloid core promoting melanin synthesis, Proceedings of the National Academy of Sciences of the United States of America, 106 (2009) 13731–13736. [PubMed: 19666488]

[19]. Puri N, Gardner JM, Brilliant MH, Aberrant pH of melanosomes in pink-eyed dilution (p) mutant melanocytes, J Invest Dermatol, 115 (2000) 607–613. [PubMed: 10998131]

[20]. Pfefferkorn CM, McGlinchey RP, Lee JC, Effects of pH on aggregation kinetics of the repeat domain of a functional amyloid, Pmel17, Proceedings of the National Academy of Sciences of the United States of America, 107 (2010) 21447–21452. [PubMed: 21106765]

[21]. McGlinchey RP, Jiang Z, Lee JC, Molecular origin of pH-dependent fibril formation of a functional amyloid, Chembiochem : a European journal of chemical biology, 15 (2014) 1569–1572. [PubMed: 24954152]

[22]. Leonhardt RM, Vigneron N, Rahner C, van den Eynde BJ, Cresswell P, Endoplasmic Reticulum Export, Subcellular Distribution, and Fibril Formation by Pmel17 Require an Intact N-terminal Domain Junction, Journal of Biological Chemistry, 285 (2010) 16166–16183. [PubMed: 20231267]

[23]. Hurbain I, Geerts WJC, Boudier T, Marco S, Verkleij AJ, Marks MS, Raposo G, Electron tomography of early melanosomes: Implications for melanogenesis and the generation of fibrillar amyloid sheets, Proceedings of the National Academy of Sciences of the United States of America, 105 (2008) 19726–19731. [PubMed: 19033461]

[24]. Jimbow M, Kanoh H, Jimbow K, Characterization of biochemical properties of melanosomes for structural and functional differentiation: analysis of the compositions of lipids and proteins in melanosomes and their subfractions, J Invest Dermatol, 79 (1982) 97–102. [PubMed: 7097043]

[25]. Jiang ZP, Lee JC, Lysophospholipid-Containing Membranes Modulate the Fibril Formation of the Repeat Domain of a Human Functional Amyloid, Pmel17, Journal of Molecular Biology, 426 (2014) 4074–4086. [PubMed: 25451784]

[26]. Kalyanasundaram K, Thomas JK, Environmental effects on vibronic band intensities in pyrene monomer fluorescence and their application in studies of micellar systems, J. Am. Chem. Soc, 99 (1977) 2039–2044.

[27]. Pedersen JS, A flux- and background-optimized version of the NanoSTAR small-angle X-ray scattering camera for solution scattering, J Appl Crystallogr, 37 (2004) 369–380.

[28]. Li YL, Beck R, Huang T, Choi MC, Divinagracia M, Scatterless hybrid metal-single-crystal slit for small-angle X-ray scattering and high-resolution X-ray diffraction, J Appl Crystallogr, 41 (2008) 1134–1139.

[29]. Schwamberger A, De Roo B, Jacob D, Dillemans L, Bruegemann L, Seo JW, Locquet JP, Combining SAXS and DLS for simultaneous measurements and time-resolved monitoring of nanoparticle synthesis, Nucl Instrum Meth B, 343 (2015) 116–122.

[30]. Debye P, Molecular-weight determination by light scattering, J Phys Colloid Chem, 51 (1947) 18–32. [PubMed: 20286386]

[31]. Koenig BW, Gawrisch K, Specific volumes of unsaturated phosphatidylcholines in the liquid crystalline lamellar phase, Biochimica et biophysica acta, 1715 (2005) 65–70. [PubMed: 16109383]

[32]. Oliver RC, Lipfert J, Fox DA, Lo RH, Doniach S, Columbus L, Dependence of Micelle Size and Shape on Detergent Alkyl Chain Length and Head Group, Plos One, 8 (2013).

[33]. Giehm L, Oliveira CL, Christiansen G, Pedersen JS, Otzen DE, SDS-induced fibrillation of alpha-synuclein: an alternative fibrillation pathway, J Mol Biol, 401 (2010) 115–133. [PubMed: 20540950]

[34]. Otzen DE, Protein-surfactant interactions: a tale of many states, Biochim. Biophys. Acta, 1814 (2011) 562–591. [PubMed: 21397738]

[35]. Stafford RE, Fanni T, Dennis EA, Interfacial Properties and Critical Micelle Concentration of Lysophospholipids, Biochemistry, 28 (1989) 5113–5120. [PubMed: 2669968]

[36]. Giehm L, Oliveira CLP, Christiansen G, Pedersen JS, Otzen DE, SDS-induced fibrillation of α-synuclein: An alternative fibrillation pathway, Journal of Molecular Biology, 401 (2010) 115–133. [PubMed: 20540950]

[37]. Kramp W, Pieroni G, Pinckard RN, Hanahan DJ, Observations on the Critical Micellar Concentration of 1-O-Alkyl-2-Acetyl-Sn-Glycero-3-Phosphocholine and a Series of Its Homologs and Analogs, Chemistry and Physics of Lipids, 35 (1984) 49–62. [PubMed: 6744496]

[38]. Kumar VV, Baumann WJ, Lanthanide-induced phosphorus-31 NMR downfield chemical shifts of lysophosphatidylcholines are sensitive to lysophospholipid critical micelle concentration, Biophys J, 59 (1991) 103–107. [PubMed: 2015376]

[39]. Meisl G, Kirkegaard JB, Arosio P, Michaels TC, Vendruscolo M, Dobson CM, Linse S, Knowles TP, Molecular mechanisms of protein aggregation from global fitting of kinetic models, Nat Protoc, 11 (2016) 252–272. [PubMed: 26741409]

[40]. Giehm L, Otzen DE, Strategies to increase the reproducibility of α-synuclein fibrillation in plate reader assays, Anal. Biochem, 400 (2010) 270–281. [PubMed: 20149780]

[41]. Giehm L, Otzen DE, Experimental approaches to inducing amyloid, in: Otzen DE (Ed.) Amyloid Fibrils and Prefibrillar Aggregates, Wiley-VCH Verlag GmbH, Place Published, 2012, pp. 295–320.

[42]. Otzen DE, Sehgal P, Westh P, α-lactalbumin is unfolded by all classes of detergents but with different mechanisms, J. Coll. Int. Sci, 329 (2009) 273–283.

[43]. Kaspersen JD, Pedersen JN, Hansted JG, Nielsen SB, Sakthivel S, Wilhelm K, Nemashkalova EL, Permyakov SE, Permyakov EA, Pinto Oliveira CL, Morozova-Roche LA, Otzen DE, Pedersen JS, Generic structures of cytotoxic liprotides: nano-sized complexes with oleic acid cores and shells of disordered proteins, Chembiochem : a European journal of chemical biology, 15 (2014) 2693–2702. [PubMed: 25403886]

[44]. De Carufel CA, Quittot N, Nguyen PT, Bourgault S, Delineating the Role of Helical Intermediates in Natively Unfolded Polypeptide Amyloid Assembly and Cytotoxicity, Angew Chem Int Ed Engl, 54 (2015) 14383–14387. [PubMed: 26440575]

[45]. Lee J, Culyba EK, Powers ET, Kelly JW, Amyloid-beta forms fibrils by nucleated conformational conversion of oligomers, Nat Chem Biol, 7 (2011) 602–609. [PubMed: 21804535]

[46]. Serio TR, Cashikar A, Kowal AS, Sawicki GJ, Moslehi JJ, Serpell L, Arnsdorf MF, Lindquist S, Nucleated conformational conversion and the replication of conformational information by a prion determinany, Science, 289 (2000) 1317–1321. [PubMed: 10958771]

[47]. Galvagnion C, Buell AK, Meisl G, Michaels TC, Vendruscolo M, Knowles TP, Dobson CM, Lipid vesicles trigger alpha-synuclein aggregation by stimulating primary nucleation, Nat Chem Biol, 11 (2015) 229–234. [PubMed: 25643172]

[48]. Campioni S, Carret G, Jordens S, Nicoud L, Mezzenga R, Riek R, The presence of an air-water interface affects formation and elongation of alpha-Synuclein fibrils, J Am Chem Soc, 136 (2014) 2866–2875. [PubMed: 24460028]

[49]. Giehm L, Otzen DE, Strategies to increase the reproducibility of protein fibrillization in plate reader assays, Anal Biochem, 400 (2010) 270–281. [PubMed: 20149780]

[50]. Otzen DE, Sehgal P, Westh P, Alpha-Lactalbumin is unfolded by all classes of surfactants but by different mechanisms, J Colloid Interface Sci, 329 (2009) 273–283. [PubMed: 18977000]

HIGHLIGHTS

- We use SAXS and ITC to investigate Pmel17 aggregation in lysolipids LPG and LPC
- LPG promotes fibrillation in a narrow concentration range, LPC only above its cmc
- Aggregation is not dependent on the cmc of LPG but on the LPG:RPT ratio
- Each RPT binds > 40 LPG, but little specific binding of LPC to RPT is detected
- LPG-RPT forms core-shell structures; no distinct LPC-RPT complexes are formed

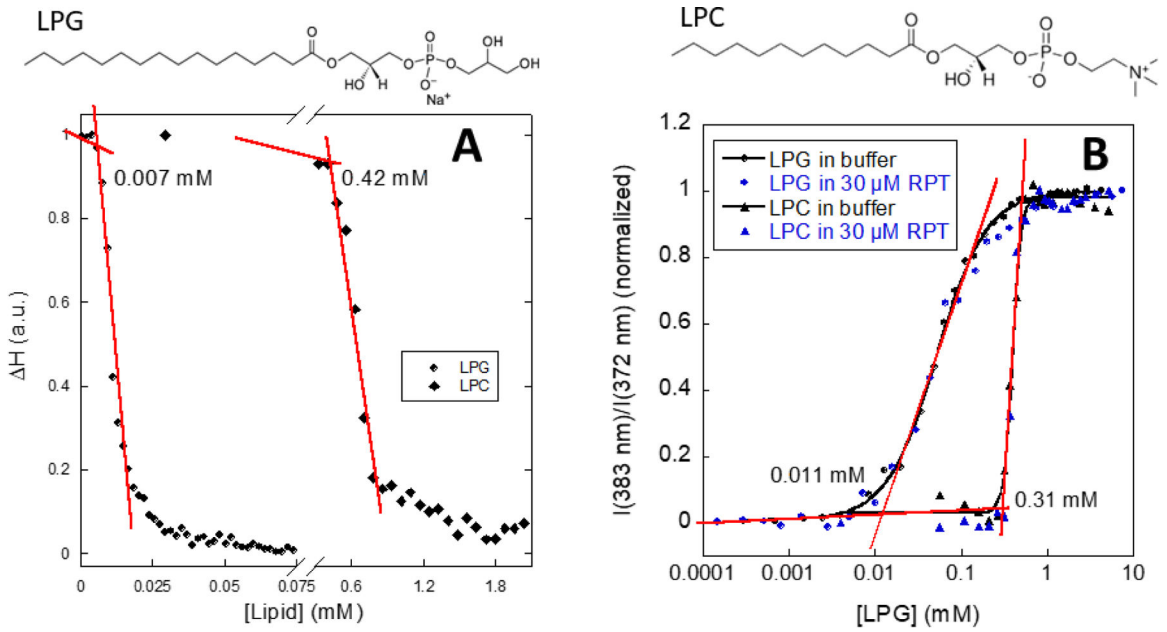

Figure 1:

(A) Enthalpogram from isothermal titration calorimetry for titration of LPG and LPC in buffer. (B) Change in fluorescence of the probe pyrene by addition of LPG/LPC in absence or presence of RPT. The structures of LPG and LPC are shown on top of the graphs.

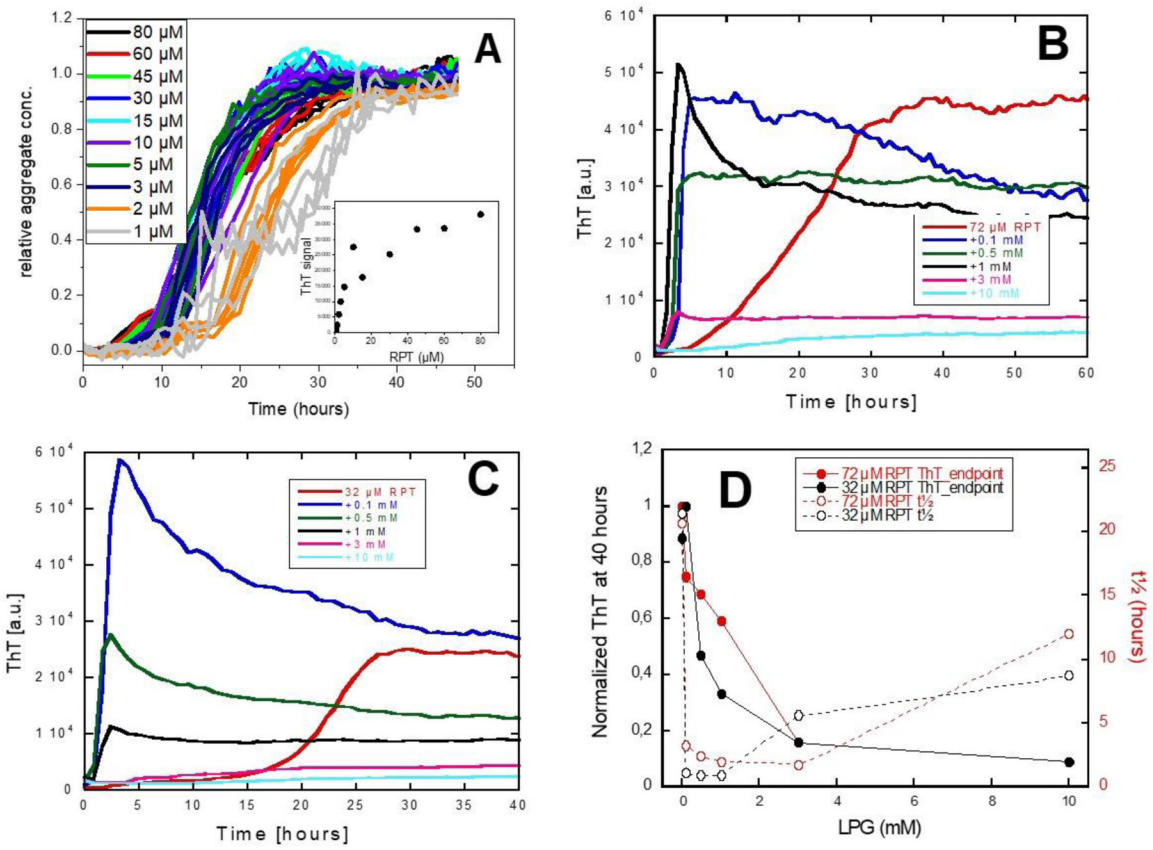

Figure 2:

ThT fluorescence profiles for RPT fibrillation with shaking at (A) 1–80 µM RPT, (B) 72 µM RPT with 0–10 mM LPG, (C) 32 µM RPT with 0–10 mM LPG and (D) ThT value at 40 hours and time for half of maximum ThT value (t1/2) for fibrillation data from (B) and (C).

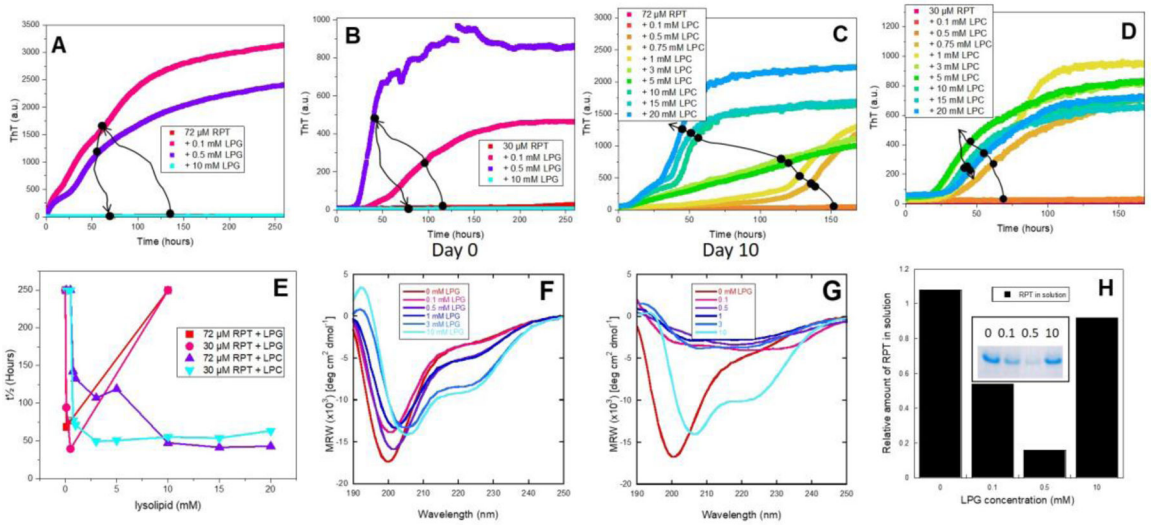

Figure 3:

ThT fluorescence profiles for RPT fibrillation without shaking at (A) 72 μM RPT with 0–10 mM LPG, (B) 30 μM RPT with 0–10 mM LPG, (C) 72 μM RPT with 0–10 mM LPC and (D) 30 μM RPT with 0–10 mM LPG. Arrows indicate data going from low to high lipid concentration. (E) t1/2 for fibrillation of RPT as a function of lysolipid concentration as determined from (A)-(D). t1/2 is set to 250 hours in cases where no fibrillation was seen in the time frame. Circular dichroism of RPT in 0–10 mM LPG (F) before and (G) after 10 days of fibrillation without shaking. (H) Amount of RPT in solution after 10 days of incubation and spin down of fibrils as determined by SDS-PAGE. Inset shows RPT bands.

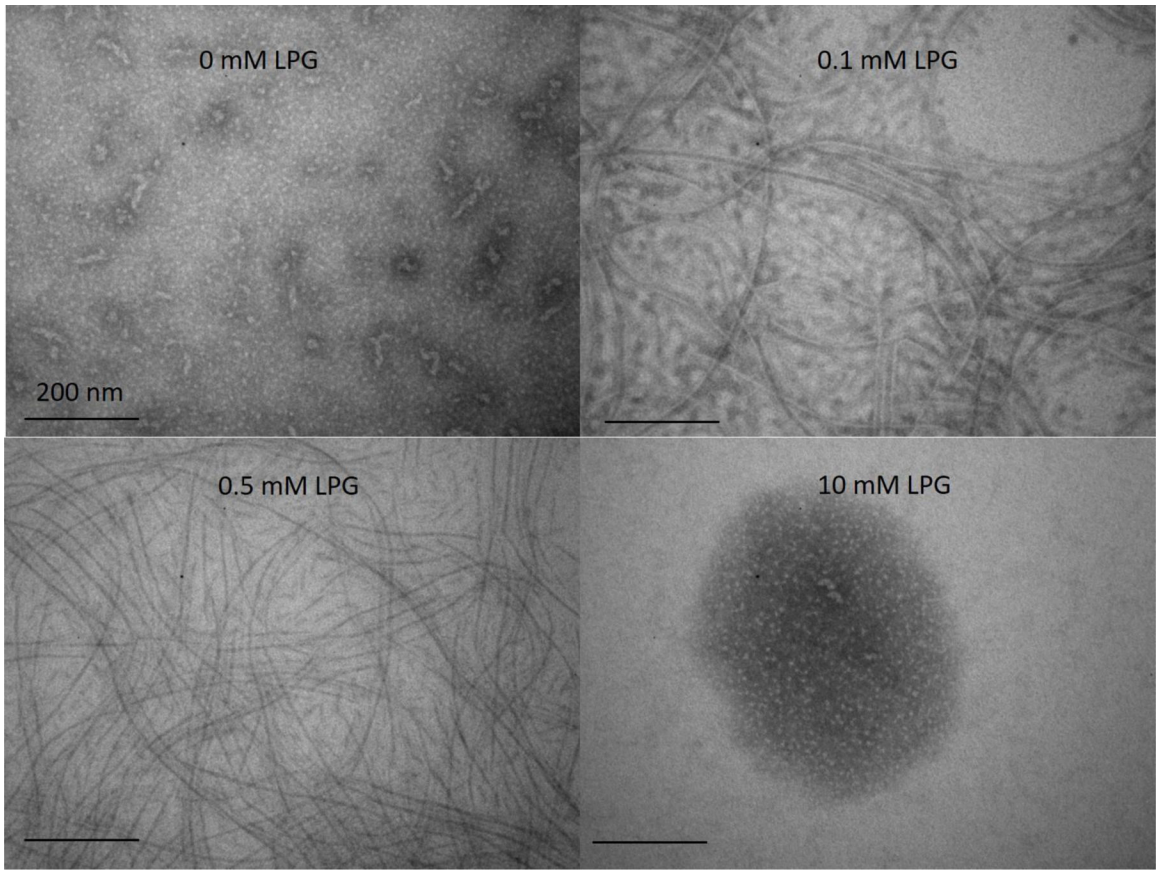

Figure 4:
Electron microscopy images of RPT samples containing 0–10 mM LPG after 10 days of incubation without shaking.

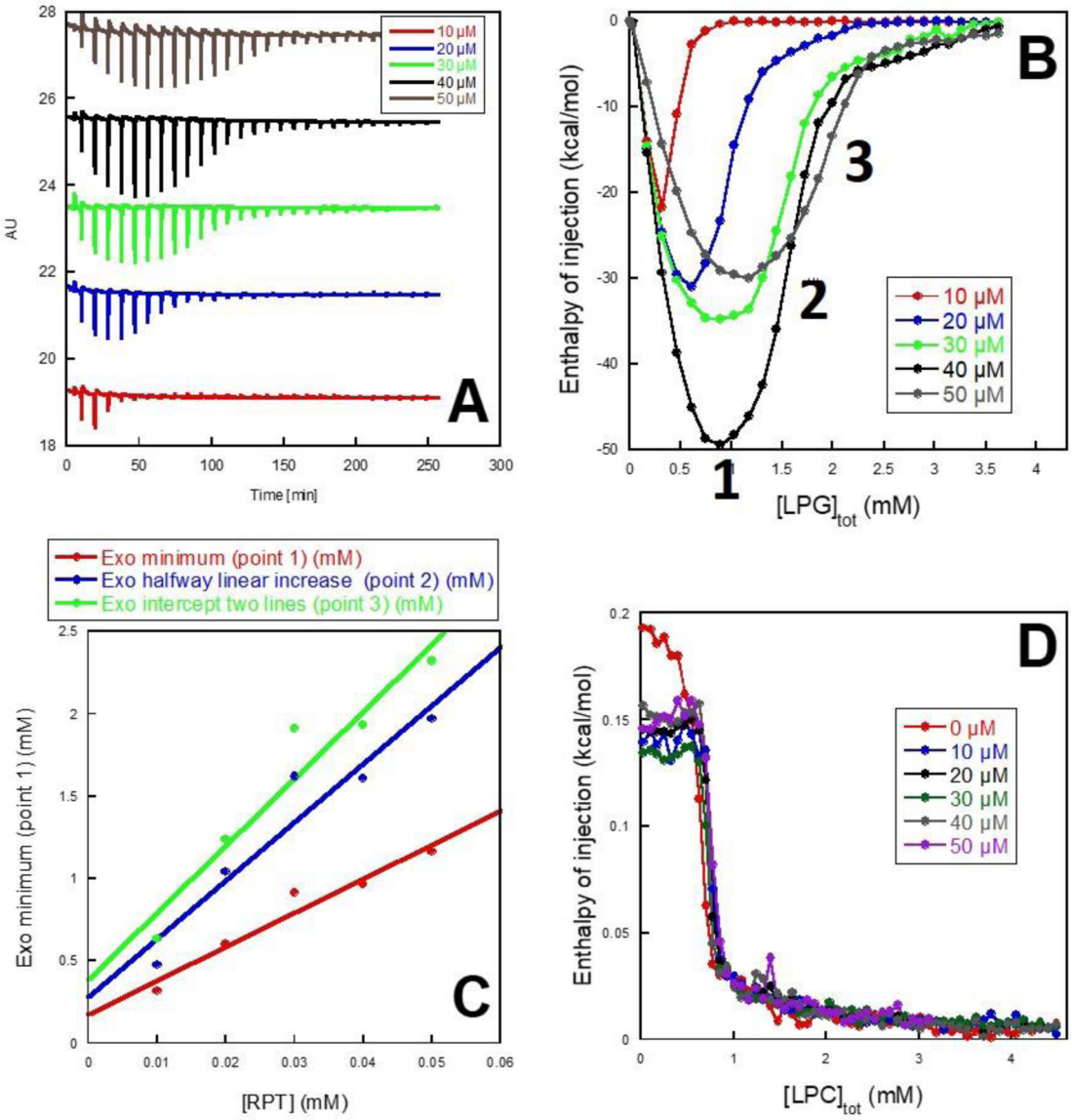

Figure 5:

(A) Titration curves from isothermal titration calorimetry. (B) Enthalpogram for titration of LPG into RPT as a function of LPG concentration. (C) LPG concentration at points 1 (The largest enthalpy change), 2 (halfway between Point 1 and baseline at 0 kcal mol^{-1}) and 3 (intercept of the two linear regions) plotted as a function of RPT concentration. A linear fit to [LPG]tot = [LPG]free + nOA,bound x [RPT] provides binding numbers. (D) Enthalpogram for titration of LPC into RPT as a function of LPC concentration.

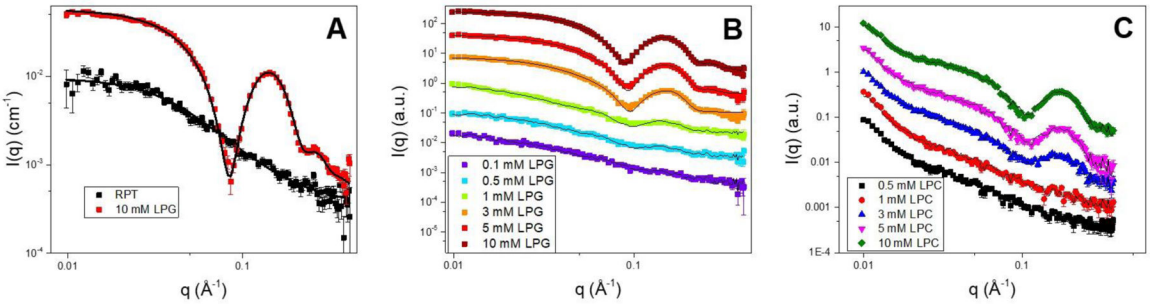

Figure 6:

(A) SAXS data of RPT and LPG. (B) SAXS data of 1 mg/ml RPT with 0.1–10 mM LPG together with model fits as described in the text. (C) SAXS data of 1 mg/ml RPT with 0.5–10 mM LPC. Samples containing 1–10 mM LPC are fitted with a linear combination of scattering for free micelles and for the sample containing 1 mg/ml + 0.5 mM LPC.

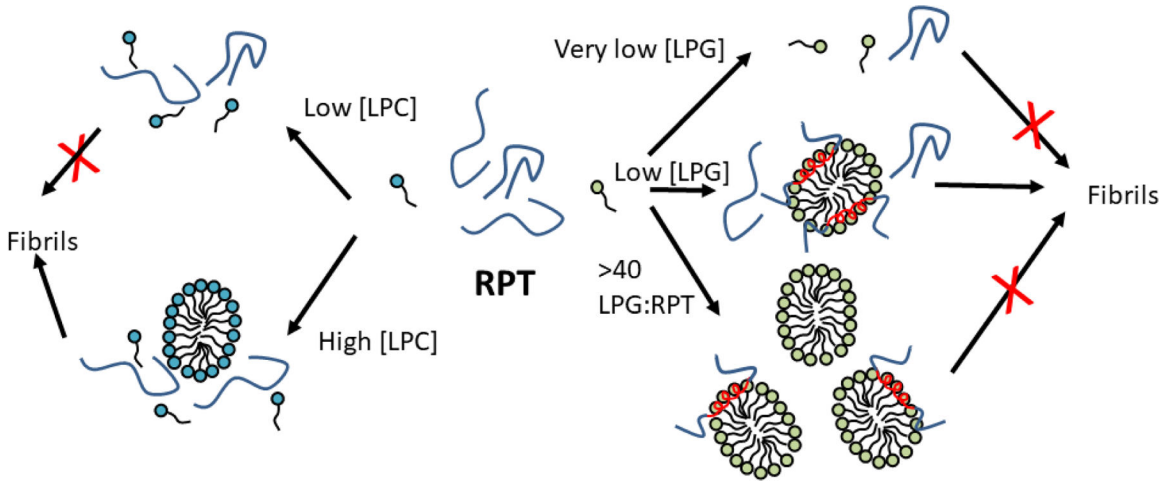

Figure 7.

Model for how the lysolipids LPG and LPC drive fibrillation of PRT in different concentration regimes. See text for details.

Table 1.

LPG-RPT binding parameters obtained from ITC experiments[a]. All data performed in 20 mM NaOAc, pH 5.0 and 100 mM NaCl at 25°C.

Characteristic point	# LPG bound per RPT[b]	$[LPG]_{free}$ (mM)[b]	$[LPG]_{total}$ (mM)[c]
Point 1	21 ± 3	0.17 ± 0.09	1.64
Point 2	36 ± 6	0.28 ± 0.21	2.80
Point 3	41 ± 7	0.39 ± 0.22	3.26

Notes:

[a] All data performed in 20 mM NaOAc, pH 5.0 and 100 mM NaCl at 25°C.

[b] Obtained from the mass balance equation $[LPG]_{tot} = [LPG]_{free} + [LPG]_{bound}[RPT]$.

[c] Calculated from a 70 μM RPT solution

Table 2

SAXS parameters obtained from fitting data to Fig. 6[a].

Conditions	χ^2	r_{core} (Å)	D_{Head} (Å)	ε	$N_{micelle}$	N_{agg}	$C_{complex}$ (mM)	$C_{free\ micelle}$ (mM)	$C_{free\ protein}$ (mg/ml)	RPT/complex
10 mM LPG	2.3	24.7 ± 0.4	9.9 ± 1.5	0.65 ± 0.01	1	95	-	-	-	-
RPT + 10 mM LPG	1.4	18.6 ± 0.9	17.3 ± 0.4	0.73 ± 0.06	1.4 ± 0.1	45	4.2 ± 0.5	5.8	-	1.1
RPT + 5.0 mM LPG	1.5	20.9 ± 0.4	16.2 ± 0.3	0.66 ± 0.02	1.4 ± 0.1	59	4.9 ± 0.5	0.1	-	1.2
RPT + 3.0 mM LPG	1.3	19.2 ± 0.4	18.0 ± 0.1	0.69 ± 0.03	1.6 ± 0.1	48	3.0	-	-	1.8
RPT + 1.0 mM LPG	1.4	16.1 ± 0.4	22.6 ± 0.7	0.70	2.9 ± 0.2	28	1.0	-	0.55 ± 0.04	2.7
RPT + 0.5 mM LPG	0.8	14.5 ± 0.4	24.1 ± 0.8	0.70	2.8 ± 0.2	21	0.5	-	0.72 ± 0.03	2.4
RPT + 0.1 mM LPG	1.1	15.6 ± 0.3	20.1 ± 3.7	0.70	13.8 ± 6.1	26	0.1	-	0.94 ± 0.03	10.3

Notes:

[a]Parameters: core radius r_{core}, shell thickness D_{Head}, micelle eccentricity ε, number of micelles $N_{micelles}$ in a cluster and number of lysolipid molecules per micelle N_{agg}. The distance between core-shell structures in clusters was set to twice the radius of the core-shell structure. Note that at high and low LPG concentrations, a term describing free LPG micelles or free proteins had to be added, respectively, to fit the data.